Indian Journal of Pure & Applied Physics
Vol. 60, April 2022, pp. 354-366

Impacts of Brownian Motion, Thermophoresis and Ohmic Heating on Chemically Reactive Pulsatile MHD Flow of Couple Stress Nanofluid in a Channel

S Rajamani[a], A Subramanyam Reddy[a,*], S Srinivas[b] & T R Ramamohan[c]

[a]Department of Mathematics, School of Advanced Sciences, Vellore Institute of Technology, Vellore-632 014, Tamil Nadu, India.
[b]Department of Mathematics, School of Advanced Sciences, VIT-AP University, Inavolu, Vijayawada – 522 237, India
[c]Department of Chemical Engineering, M S Ramaiah Institute of Technology, Bangalore- 560 054, India.

Received 16 September 2021; accepted 23 March 2022

In this study, the magnetohydrodynamic pulsatile flow of a couple stress nanofluid in a channel has been discussed in detail by adopting Buongiorno's nanofluid model. The impacts of Brownian motion, thermophoresis, Ohmic heating, viscous dissipation and chemical reaction on heat, and mass transfer of blood based nanofluid are considered. The current concept is significant in the field of nano-drug supply, dynamics of physiological fluids, and biomedicines. The governing partial differential equations are converted into a set of ODEs (ordinary differential equations) by employing a perturbation scheme. The resulting non-dimensional system is numerically interpreted to determine the impact of various emerging parameters on flow variables by utilizing the shooting technique with the support of the Runge-Kutta procedure. The outcomes reveal that the temperature rises with the magnifying viscous dissipation, Brownian motion, and thermophoresis parameters, whereas the opposite trend can be seen with an escalation in the couple stress parameter. Heat transfer rate is an accelerating function of Brownian motion and thermophoresis parameters while it is a decelerating function of couple stress parameter and Hartmann number. Mass transfer rate declines with increasing values of thermophoresis parameter and Lewis number.

Keywords: Pulsatile flow; Couple stress nanofluid; Thermophoresis; Brownian motion parameter; Thermal radiation

1 Introduction

Nanoparticles in conventional thermal transport fluids endeavour to attain the optimum thermo-physical character at the minimum promising concentrations via uniform distribution and persistence, which is a feature of a nanofluid. Nanofluids have promising applications in science and engineering like air conditioning and cooling systems, portable supercomputers, drug supply, crystal formation, food biophysics, carcinogenic treatment, solar absorption, and biomedicines[1-10]. Buongiorno[11] initiated the generalized non - homogenous paradigm for transportation in nanofluids with two phases with the consideration of Brownian motion and thermophoresis effects. Nield and Kunzov[12] analytically studied the fully developed laminar forced convective nanofluid flow in a parallel plate channel with a permeable medium by adopting the influences of thermo-phoresis and Brownian movement. Srinivas *et al*.[13] analytically investigated the influences of magnetic parameter and heat generation/absorption parameter on nanofluid flow in a porous pipe by utilizing the homotopy analysis method. Makinde and Eegunjobi[14] examined the heat (Nusselt number) and mass (Sherwood number) transfer characteristics of a couple stress nanofluid flow in a penetrable channel under the consideration of radiative heat and magnetic parameters. Uddin *et al.*[15] numerically explored the model for the bio nanomaterials processing with an investigation of hydromagnetic boundary layer slip flow of an electrically treated nanofluid in an expanding/ contracting sheet by employing the Runge-Kutta Fehlberg fourth fifth-order method. Chaudhary and Chouhan[16] inspected the hydromagnetic slip flow of Cu-blood nanofluid past an extendable surface with the effects of Ohmic and viscous dissipations by utilizing the numerical technique. Rana *et al.*[17] considered the problem of an electrically conducting nanofluid flow in a penetrable cavity with the involvement of radiative heat and a slanted magnetic field. Shamshuddin and Eid[18] have carried out an extensive analysis of an unparalleled heat source (or sink), viscous dissipation, thermophoresis, Ohmic heating, Brownian motion, and the 1st order chemical processes on the flow of nth order reactive nanofluids over an extendable sheet using a numerical approach.

*Corresponding author:
(E-mail: anala.subramanyamreddy@gmail.com)

In many research and manufacturing processes, the heat and mass transfer of non-Newtonian fluid flow is seen leading to interest in the study of non-Newtonian fluids. One of the important models of non-Newtonian fluid models is the couple stress fluid model which is very useful in industries and engineering like polymeric materials or dissolvent, synthesized fluids, biological fluids, fluid crystal, and lubricants[19-23]. Stokes[24] pioneered the concept of a couple stress fluid for the magnetohydrodynamic channel flows. Sithole *et al*.[25] modeled the hydromagnetic couple stress nanofluid flow with the combined effects of a chemical reaction and radiative heat to analyze the heat and mass transfer by adopting a numerical simulation. Salman and Abdulhadi[26] interpreted the peristaltic flow of a non-Newtonian fluid with couple stress in an inclined channel with the impacts of heat and mass transfer by employing a numerical scheme. Rosales *et al*.[27] investigated the flow of a couple stress nanofluid in a penetrable channel with the effects of radiative heat and magnetic parameter by adopting the shooting technique along with the Runge-Kutta procedure. Subramaniam and Mondal[28] developed the updated linear Maxwell framework under the action of couple stress with the first concepts of thermodynamics using a power model for the kinetics and rheology of viscoelastic fluids. Aziz *et al*.[29] employed Buongiorno's nanofluid model to elucidate the novel characteristics of Brownian motion and thermophoresis on the flow of a chemically reacting couple stress nanofluid on the two-directional periodically extended surface with the aid of the homotopy analysis method. Roja and Gireesha[30] have carried out a theoretical investigation on the flow of a hydromagnetic couple stress nanofluid in a slanted channel under the influence of a radiative heat and heat source by utilizing numerical scrutinization. Rajamani and Reddy[31] analytically studied the magnetohydrodynamic pulsatile flow of a couple stress nanofluid via channel with the effects of Joule heating and radiative heat by using the perturbation technique.

The analysis of pulsatile flow in a channel or pipe is significant to a number of natural activities in the human body, other natural systems, industrial, engineering, biological fluids, and physiological processes[32-39] which are sensitive to fluctuations in pressure gradient. Wang[40] analyzed the axial pulsating flow motivated by the axial pressure driven gradient on the penetrable channel with the impacts of magnetic parameter and crossflow Reynolds number. Radha krishnamacharya and Maiti[41] inspected the rate of energy transport on pulsating flow in a permeable channel and highlighted this as the key factor in the dialysis of blood in the artificial kidney. Bestman[42] discussed the pulsating flow which is induced with the pressure driven gradient on the slanted heat permeable channel. Adesanya and Makinde[43] presented the heat transfer distributions for the pulsating flow on a magneto couple stress fluid on the penetrable channel with the consideration of radiative heat and applied magnetic field. Ahmed and Xu[44] analytically examined the unsteady pulsatile flow of copper-alumina-water hybrid nanofluid driven in a microchannel with the consideration of magnetic parameter and radiative heat impacts. Kumar *et al*.[45] attempted to study the pulsating flow of a non-Newtonian fluid on the penetrable channel under the influences of Ohmic heating, radiative heat, and magnetic parameter by using the Buongiorno model with a numerical scheme. Ali *et al*.[46] addressed the influence of an applied magnetic field on the pulsating flow of non-Newtonian Casson fluid in a restrained channel by a numerical investigation. Venkatesan and Reddy[47] analytically investigated the pulsatile flow of a non-Newtonian Oldroyd-B nanofluid in a channel with viscous dissipation, Ohmic heating, and thermal radiation by adopting the perturbation technique. Esfe *et al*.[48] critically reviewed the applications of pulsatile flow in traditional heat transfer fluids and novel nanofluids by the inspection on heat and hydraulic features of nanofluids and conventional heat transfer fluids. Venkatesan and Reddy[49] analytically explored the impact of Ohmic heating on hydromagnetic pulsative flow of blood based non Newtonian nanofluid in a penetrable channel with the aid of perturbation method.

In the light of important applications in science and engineering like polymer processes, power generation, aircraft dynamics, geological process, plastic films, dye extruding, and glass bowling[50-53] there is a lot of scope for studies of thermal radiation together with viscous and Ohmic dissipations. Vijayaraghavan *et al*.[54] inspected the impacts of radiative heat on the MHD Casson fluid flow with the consideration of heat generation/absorption past an inclined layer by employing the Laplace transform technique. Sheikholeslami and Shehsaz[55] selected a numerical approach to investigate the impact of radiative heat on nanofluid flow with the presence of Lorentz forces by adopting the Maxwell-Garnett

method. Sheikholeslami and Rokni[56] reported the effect of thermal radiation on a nanofluid character through a numerical procedure. Reddy *et al*.[57] focused on the impact of radiative heat, viscous, and Ohmic dissipations on a couple stress fluid in a slanted channel with the effect of the chemical reaction by employing the numerical procedure. Shoiab *et al*.[58] numerically explored the effect of radiative heat, viscous dissipation, and Joule heating on the radiative flow of nanofluid past a rotational disk. Ali *et al*.[59] demonstrated the numerical procedure of the radiative heated pulsating flow of a nanofluid in a narrow channel for the model of blood flow in arteries.

The above literature survey reveals that there is no study of the pulsatile hydromagnetic flow of couple stress nanofluid via channel along with the presence of Brownian motion, thermo-phoresis, and thermal radiation so far. The main goal of this work is to investigate the pulsatile flow of magnetohydrodynamic couple stress nanofluid in a channel with the Buongiorno nanofluid model. The influences of Ohmic heating, viscous dissipation, Brownian motion, thermophoresis, and thermal radiation are considered. The flow transport partial differential equations (PDEs) are converted into ODEs by employing the perturbation technique, then solved by utilizing the shooting technique along with the support of the Runge-Kutta 4th order procedure. The profiles of velocity, temperature, and concentration distributions for the emerging parameters are displayed with the aid of pictorial results and discussed in detail.

2 Formulation of the problem

In this investigation, an incompressible, laminar, electrically conducting pulsatile flow of a couple stress nanofluid via channel is considered. In this investigation, blood is considered as a couple stress fluid. The impacts of thermo-phoresis, Brownian movement, viscous dissipation, Ohmic heating, and chemical reaction are taken into account. The schematic diagram of the current flow is presented in Fig. 1. The x^*-axis coincides with the bottom wall while the y^*- axis is perpendicular to both walls. An applied magnetic field of magnitude B_0 is applied uniformly orthogonal to the walls. T_1 and T_0 are the wall temperatures of top and bottom walls accordingly $(T_0 < T_1)$, C_1 and C_0 are the nanoparticles concentrations of top and bottom walls respectively

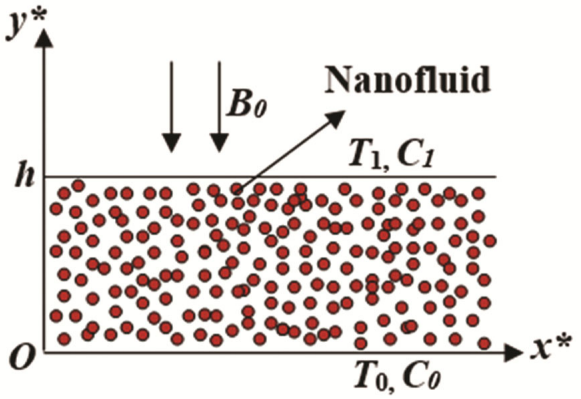

Fig. 1 — Flow model of the problem.

$(C_0 < C_1)$, and h is the distance between the walls. We assume the flow is induced by the pulsatile pressure driven gradient. So, the pressure driven gradient is taken in[40-41]

$$-\frac{1}{\rho_f}\frac{\partial P^*}{\partial x^*} = A(1+\varepsilon\exp(i\omega t^*)), \qquad \ldots(1)$$

here, P^* is the fluid pressure, ω is the frequency, $\varepsilon(<<1)$ is a positive quantity, t^* is time, and A is a constant. Under these hypotheses the governing equations of the current study are

$$\rho_f\frac{\partial u^*}{\partial t^*} = -\frac{\partial P^*}{\partial x^*} + \mu_f\left(\frac{\partial^2 u^*}{\partial y^{*2}}\right) - \eta\frac{\partial^4 u^*}{\partial y^{*4}} - \sigma_f B_0{}^2 u^*, \qquad \ldots(2)$$

$$\frac{\partial T^*}{\partial t^*} = \frac{k_f}{\left(\rho C_p\right)_f}\frac{\partial^2 T^*}{\partial y^{*2}} + \tau D_B\left(\frac{\partial C^*}{\partial y^*}\frac{\partial T^*}{\partial y^*}\right) + \tau\frac{D_T}{T_m}\left(\frac{\partial T^*}{\partial y^*}\right)^2 + \frac{\mu_f}{\left(\rho C_p\right)_f}\left(\frac{\partial u^*}{\partial y^*}\right)^2 + \frac{\eta}{\left(\rho C_p\right)_f}\left(\frac{\partial^2 u^*}{\partial y^{*2}}\right)^2 - \frac{1}{\left(\rho C_p\right)_f}\frac{\partial q_r{}^*}{\partial y^*} + \frac{Q_0}{\left(\rho C_p\right)_f}\left(T^* - T_0\right) + \frac{\sigma_f B_0{}^2}{\left(\rho C_p\right)_f}u^{*2}, \qquad \ldots(3)$$

$$\frac{\partial C^*}{\partial t^*} = D_B\frac{\partial^2 C^*}{\partial y^{*2}} + \frac{D_T}{T_m}\left(\frac{\partial^2 T^*}{\partial y^{*2}}\right) - k_1 C^* \qquad \ldots(4)$$

here u^* is the velocity component of x^* direction, μ_f, ρ_f, $(\rho C_p)_f$, σ_f, k_f represent the viscosity, density, heat capacitance, electrical conductivity, and thermal conductivity of the base fluid. T^*, C^* are the temperature and concentration of the fluid, $\tau = (\rho C_p)_p / (\rho C_p)_f$, $(\rho C_p)_p$ is an effective specific heat of nanoparticles. Q_0 is coefficient of heat generation/absorption, η is the coefficient of couple stress viscosity, and q_r is thermal radiative flux. k_1 is the first-order chemical reaction rate, T_m is the mean temperature, D_T is the coefficient of diffusive thermophoresis, and D_B is the coefficient of diffusive Brownian movement.

The related B.Cs (boundary conditions) are,

$$\begin{aligned} &u^*(0)=0,\ \frac{\partial^2 u^*}{\partial y^{*2}}(0)=0,\ T^*(0)=T_0,\\ &C^*(0)=C_0,\ u^*(h)=0,\frac{\partial^2 u^*}{\partial y^{*2}}(h)=0,\\ &T^*(h)=T_1,\ C^*(h)=C_1. \end{aligned} \qquad \ldots(5)$$

By adopting Rosseland estimation for radiative thermal flux (q_r), equation (3) becomes,

$$\begin{aligned} \frac{\partial T^*}{\partial t^*} &= \frac{k_f}{(\rho C_p)_f}\frac{\partial^2 T^*}{\partial y^{*2}} + \tau D_B\left(\frac{\partial C^*}{\partial y^*}\frac{\partial T^*}{\partial y^*}\right)\\ &+\tau\frac{D_T}{T_m}\left(\frac{\partial T^*}{\partial y^*}\right)^2 + \frac{16\sigma^* T_1^3}{3(\rho C_p)_f k^*}\frac{\partial^2 T^*}{\partial y^{*2}}\\ &+\frac{\eta}{(\rho C_p)_f}\left(\frac{\partial^2 u^*}{\partial y^{*2}}\right)^2 + \frac{\mu_f}{(\rho C_p)_f}\left(\frac{\partial u^*}{\partial y^*}\right)^2\\ &+\frac{Q_0}{(\rho C_p)_f}(T^*-T_0)+\frac{\sigma_f B_0^{\,2}}{(\rho C_p)_f}u^{*2}. \end{aligned} \qquad \ldots(6)$$

Here k^* is the Rosseland mean absorption coefficient, and σ^* is the Stephen-Boltzmann constant

Now, with the help of the below non-dimensional parameters and variables,

$$\left.\begin{aligned} &x^*=xh,\ y^*=yh,\ t^*=\frac{t}{\omega},\ u^*=\frac{Au}{\omega},\ P^*=\rho_f PAh,\\ &T^*=T_0+\theta(T_1-T_0), C^*=C_0+\phi(C_1-C_0),\ H=\frac{(\omega)^{1/2}h}{(\upsilon_f)^{1/2}},\ M=B_0 h\left(\frac{\sigma_f}{\mu_f}\right)^{1/2},\\ &\Pr=\frac{\upsilon_f(\rho Cp)_f}{k_f},\ Ec=\frac{A^2}{\omega^2(C_p)_f(T_1-T_0)},\ \lambda=\frac{\eta}{\mu_f h^2},\\ &Rd=\frac{4\sigma^* T_1^3}{k^* k_f},\ Q=\frac{Q_0 h^2}{\upsilon_f(\rho Cp)_f},\ N_b=\frac{\tau D_B(C_1-C_0)}{\upsilon_f},\\ &N_t=\frac{\tau D_T(T_1-T_0)}{T_m\upsilon_f},\ Le=\frac{k_f}{(\rho Cp)_f D_B},\\ &\gamma=\frac{k_1 h^2}{\upsilon_f},\ K_1=\frac{k_1 C_0 h^2}{\upsilon_f(C_1-C_0)}, \end{aligned}\right\} \qquad \ldots(7)$$

equations (1), (2), (4), and (6) become

$$-\frac{\partial P}{\partial x} = 1+\varepsilon\exp(it), \qquad \ldots(8)$$

$$\frac{\partial u}{\partial t} = -\frac{\partial P}{\partial x}+\frac{1}{H^2}\left(\frac{\partial^2 u}{\partial y^2}\right)-\frac{\lambda}{H^2}\frac{\partial^4 u}{\partial y^4}-\frac{M^2}{H^2}u, \qquad \ldots(9)$$

$$\begin{aligned} \frac{\partial\theta}{\partial t} &= \frac{\left(1+\frac{4}{3}Rd\right)}{\Pr H^2}\left(\frac{\partial^2\theta}{\partial y^2}\right)+\frac{N_b}{H^2}\left(\frac{\partial\phi}{\partial y}\frac{\partial\theta}{\partial y}\right)\\ &+\frac{N_t}{H^2}\left(\frac{\partial\theta}{\partial y}\right)^2+\frac{Ec}{H^2}\left(\frac{\partial u}{\partial y}\right)^2\\ &+\frac{\lambda Ec}{H^2}\left(\frac{\partial^2 u}{\partial y^2}\right)^2+\frac{EcM^2}{H^2}u^2+\frac{Q}{H^2}\theta, \end{aligned} \qquad \ldots(10)$$

$$\begin{aligned} \frac{\partial\phi}{\partial t} &= \frac{1}{Le\Pr H^2}\frac{\partial^2\phi}{\partial y^2}+\frac{1}{Le\Pr H^2}\frac{N_t}{N_b}\left(\frac{\partial^2\theta}{\partial y^2}\right)\\ &-\frac{\gamma}{H^2}\phi-\frac{K_1}{H^2}, \end{aligned} \qquad \ldots(11)$$

here Ec is the Eckert number, M is Hartmann number, $\Pr$ is the Prandtl number, Q is the heat source/sink parameter, H is frequency parameter, Rd is radiation parameter, λ is couple stress parameter, Le is Lewis number, and γ is the chemical reaction parameter.

The corresponding B.Cs are

$$\left.\begin{aligned} &u(0)=0,\ \frac{\partial^2 u}{\partial y^2}(0)=0,\ \theta(0)=0,\ \phi(0)=0,\\ &u(1)=0,\ \frac{\partial^2 u}{\partial y^2}(1)=0,\ \theta(1)=1,\ \phi(1)=1. \end{aligned}\right\} \qquad \ldots(12)$$

3 Solution of the problem

On account of eqn. (8), the resulting expressions for u, θ, and ϕ are

$$u(y) = u_0(y) + \varepsilon u_1(y)\exp(it), \quad \ldots(13)$$

$$\theta(y) = \theta_0(y) + \varepsilon\theta_1(y)\exp(it), \quad \ldots(14)$$

$$\phi(y) = \phi_0(y) + \varepsilon\phi_1(y)\exp(it). \quad \ldots(15)$$

By substituting Eqs. (8), (13)-(15) into the Eqs. (9)-(11) and then equating the coefficients of different powers of ε, one obtains

$$\lambda\frac{d^4u_0}{dy^4} - \frac{d^2u_0}{dy^2} + M^2u_0 = H^2, \quad \ldots(16)$$

$$\lambda\frac{d^4u_1}{dy^4} - \frac{d^2u_1}{dy^2} + (iH^2 + M^2)u_1 = H^2, \quad \ldots(17)$$

$$\begin{aligned}&\frac{\left(1+\frac{4}{3}Rd\right)}{\Pr}\frac{d^2\theta_0}{dy^2} + N_b\left(\frac{d\theta_0}{dy}\frac{d\phi_0}{dy}\right)\\ &+ N_t\left(\frac{d\theta_0}{dy}\right)^2 + Q\theta_0 + \lambda Ec\left(\frac{d^2u_0}{dy^2}\right)^2\\ &+ Ec\left(\frac{du_0}{dy}\right)^2 + EcM^2{u_0}^2 = 0,\end{aligned} \quad \ldots(18)$$

$$\begin{aligned}&\frac{\left(1+\frac{4}{3}Rd\right)}{\Pr}\frac{d^2\theta_1}{dy^2} + N_b\left(\frac{d\phi_0}{dy}\frac{d\theta_1}{dy} + \frac{d\phi_1}{dy}\frac{d\theta_0}{dy}\right)\\ &+ 2N_t\left(\frac{d\theta_0}{dy}\frac{d\theta_1}{dy}\right) + (Q - iH^2)\theta_1\\ &+ 2\lambda Ec\frac{d^2u_0}{dy^2}\frac{d^2u_1}{dy^2} + 2Ec\frac{du_0}{dy}\frac{du_1}{dy}\\ &+ 2EcM^2u_0u_1 = 0,\end{aligned} \quad \ldots(19)$$

$$\frac{1}{Le\Pr}\frac{d^2\phi_0}{dy^2} + \frac{1}{Le\Pr}\frac{N_t}{N_b}\frac{d^2\theta_0}{dy^2} - \gamma\phi_0 + K_1 = 0, \quad \ldots(20)$$

$$\begin{aligned}&\frac{1}{Le\Pr}\frac{d^2\phi_1}{dy^2} - (\gamma + iH^2)\phi_1\\ &+ \frac{1}{Le\Pr}\frac{N_t}{N_b}\frac{d^2\theta_1}{dy^2} = 0.\end{aligned} \quad \ldots(21)$$

The corresponding B.Cs are

$$\begin{aligned}&u_0(0) = 0,\ u_1(0) = 0,\ \frac{d^2u_0}{dy^2}(0) = 0,\\ &\frac{d^2u_1}{dy^2}(0) = 0,\ \theta_0(0) = 0,\ \theta_1(0) = 0,\\ &\phi_0(0) = 0,\ \phi_1(0) = 0,\ u_0(1) = 0,\\ &u_1(1) = 0,\ \frac{d^2u_0}{dy^2}(1) = 0,\ \frac{d^2u_1}{dy^2}(1) = 0,\\ &\theta_0(1) = 1,\ \theta_1(1) = 0,\ \phi_0(1) = 1,\ \phi_1(1) = 0.\end{aligned} \quad \ldots(22)$$

Further, the rates of heat (Nusselt number) and mass (Sherwood number) transfer at both walls are delineated as[41,45]

$$Nu = \left(\frac{\partial\theta}{\partial y}\right)_{y=0,1},\ Sh = \left(\frac{\partial\phi}{\partial y}\right)_{y=0,1} \quad \ldots(23)$$

Now, the set of equations (16)-(21) are solved by adopting the shooting technique with the support of the Runge-Kutta fourth-order procedure.

4 Result and discussion

The system of Eqs. (16)-(21) along with the B.Cs (22) are deciphered numerically by adopting Runge-Kutta 4th order scheme with the aid of the shooting procedure. The step size is fixed as 0.001 (i.e. $\Delta y = 0.001$) precision is static for the convergence criteria. In this section the pictorial results are portrayed to see the effects of various parameters such as Eckert number Ec, Hartmann number M, couple stress parameter λ, radiation parameter Rd, heat source/sink parameter Q, time t, frequency parameter H, Brownian movement parameter Nb, thermophoresis parameter Nt, chemical reaction parameter γ, and Lewis number Le on velocity, temperature and concentration distributions in Figs. 2-9. In this analysis, u_t, θ_t, ϕ_t represent unsteady velocity, unsteady temperature, and unsteady concentration of nanoparticles of couple stress nanofluid accordingly. For the present analysis, the considered values of various dimensionless parameters are $Q = -0.5$, $\varepsilon = 0.001$, $\lambda = 0.2$, $M = 2$, $H = 2$, $Rd = 1$, $\Pr = 21$, $Ec = 0.6$, $Nb = 0.5$, $Nt = 0.5$, $\gamma = 1$, $Le = 1$, $K_1 = 0.001$, $t = \pi/4$, and for unsteady temperature distribution, $Q = -0.1$ unless otherwise stated.

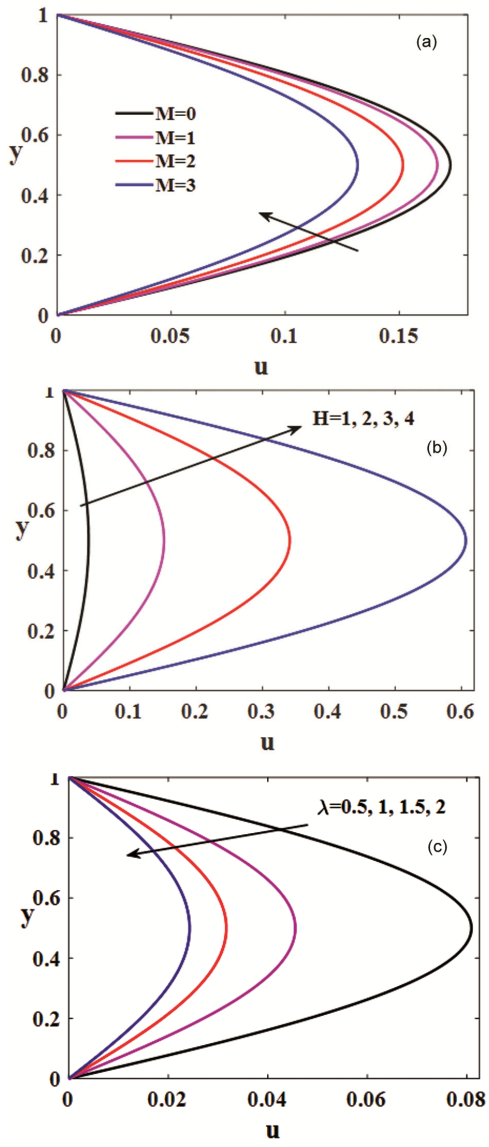

Fig. 2 — Velocity distribution (a) impact of M =0, 1, 2, 3, (b) impact of H =1, 2, 3, 4, (c) impact of λ =0.5, 1, 1.5, 2.

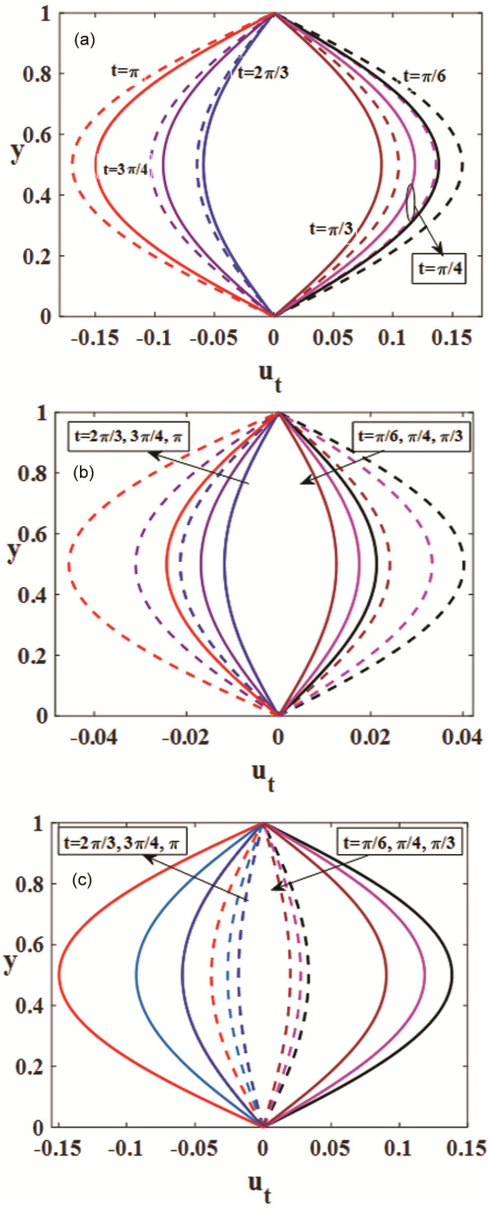

Fig. 3 — (a) Effect of M and $t = \frac{\pi}{6}, \frac{\pi}{4}, \frac{\pi}{3}, \frac{2\pi}{3}, \frac{3\pi}{4}, \pi$, dashed line M=0, solid line M =2, (b) impact of λ and $t = \frac{\pi}{6}, \frac{\pi}{4}, \frac{\pi}{3}, \frac{2\pi}{3}, \frac{3\pi}{4}, \pi$, dashed line λ =1, solid line λ =2, (c) impact of H and $t = \frac{\pi}{6}, \frac{\pi}{4}, \frac{\pi}{3}, \frac{2\pi}{3}, \frac{3\pi}{4}, \pi$, dashed line H =1, solid line H =2, on unsteady velocity distribution.

The profiles of velocity distribution for various values of M, H, and λ are displayed in Figs. 2(a-c). Fig. 2(a) elucidates that the velocity is decelerating with a rise in M. This decrease in velocity is because of the delaying forces created by the applied magnetic field which act reverse to the flow path and result in a reduction in the velocity of a couple stress nanofluid. Fig. 2(b) elucidates that the velocity of nanofluid is an increasing function H. From Fig. 2(c), one can infer that there is a deceleration in velocity of couple stress nanofluid for increasing values of couple stress parameter. Figs. 3(a-c) display the impacts of M, λ, and H for various t values. From these same figures, it is noticed that the velocity distribution oscillates with time t and the maximum velocity is near to the center of the channel. An increment in the Hartmann

number leads to the decrement in velocity distribution of nanofluid because the Lorentz forces (generated by the applied magnetic field) act opposite to the flow path which is noticed from Fig. 3(a). From Fig. 3(b), it is evident that u_t is a declining function of λ while it is a growing function of H see Fig.3(c).

Figures. 4(a-d) display the effects of Ec, M, λ, and H on θ. From Fig. 4(a), it can be seen that magnifying viscous dissipation (Eckert number) increases the temperature of a couple stress nanofluid which is due to the uplifting Ec dissipating more heat (frictional heating) in the fluid, this boosts up the temperature of the current working fluid. Fig. 4(b) portrays that increasing the Hartmann number leads to declining the temperature of the fluid which is due to the applied magnetic field retarding the flow of couple stress nanofluid. The impact of λ on the distributions of θ is delineated in Fig. 4(c). This figure illustrates that temperature is a diminishing function of a couple stress parameter. Fig. 4(d) elucidates that there is a rise in temperature of the nanofluid with the high values of frequency parameter.

Figures. 5(a-d) depict the effects of Nb, Nt, Q, and Rd on θ. Fig. 5(a) shows the temperature variations for the various values of Nb. It is clear that there is a significant escalation in the temperature of the nanofluid which is because the Brownian motion has a tendency to heat the fluid (*i.e.* increasing Brownian motion increase the random movement of particles). The influence of Nt on temperature distribution of the nanofluid is captured in Fig. 5(b). This figure explains that the thermophoretic impact encourages the immigration of nanoparticles from the hot region to the fluid which clues to the rise in temperature of the fluid. Fig. 5(c) is depicted to elevate the influence of Q on temperature variations of the nanofluid, it is evident that the temperature is increasing with the uplifting values of heat source $(Q > 0)$, which is due to the heat generation in the fluid, whereas quite opposite behaviour can be found for the high values of the heat sink $(Q < 0)$, which is due to the heat amalgamation in the fluid. Fig. 5(d) shows that the temperature of couple stress fluid is increasing for rising values of radiation parameter, which is due to the radiation parameter making a contribution to the heat diffusion of conductive heat in the heat absorption part.

Figures. 6(a-d) display the possessions of Ec, M, λ, and H on θ_t. From these pictorial outcomes, it is noticed that the unsteady temperature distributions exhibit wavering nature and the maximum is near the lower wall. From Fig. 6(a), it can be seen that increasing viscous dissipation enhances θ_t due to the heat generated by viscous dissipation and the maximum of θ_t is near to the lower wall. Fig. 6(b)

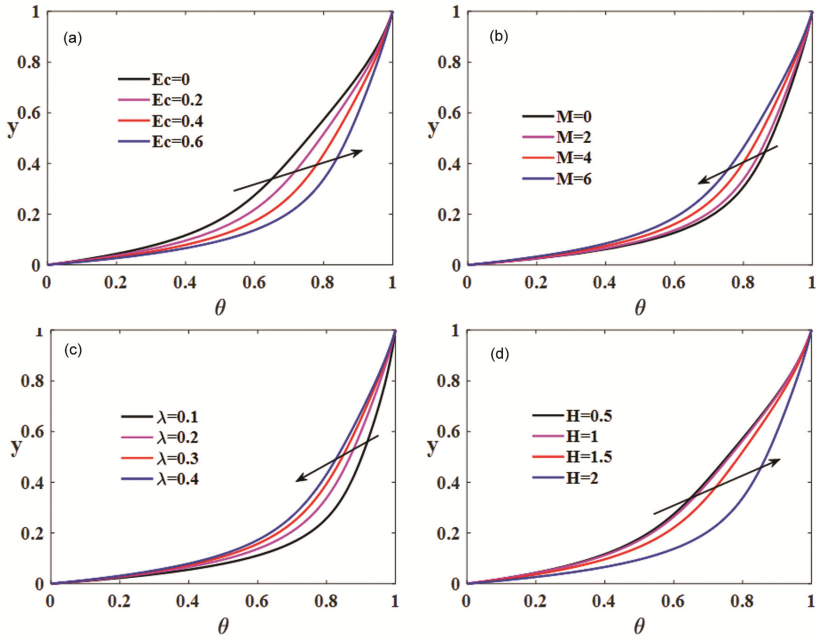

Fig. 4 — (a) Influence of Ec =0, 0.2, 0.4, 0.6, on θ, (b) influence of M =0, 2, 4, 6, on θ, (c) influence of λ =0.1, 0.2, 0.3, 0.4, on θ, (d) influence of H =0.5, 1, 1.5, 2, on θ.

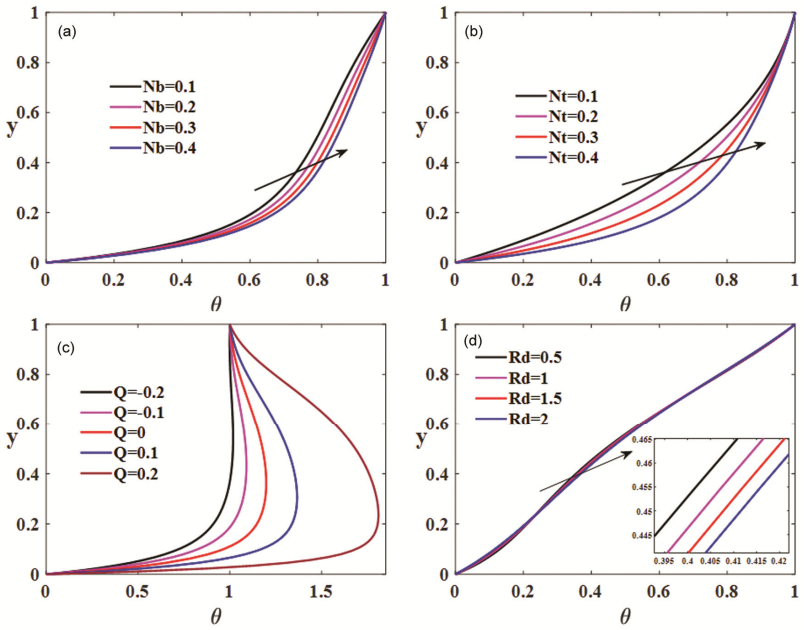

Fig. 5 — (a) Impression of Nb =0.1, 0.2, 0.3, 0.4, on θ when $Q=-0.5$, (b) impact of Nt =0.1, 0.2, 0.3, 0.4, on θ when $Q=-0.5$, (c) impact of Q =-0.2, -0.1, 0, 0.1, 0.2, on θ when $Q=-0.5$, (d) impact of Rd =0.5, 1, 1.5, 2, on θ when $Q=-2.5$.

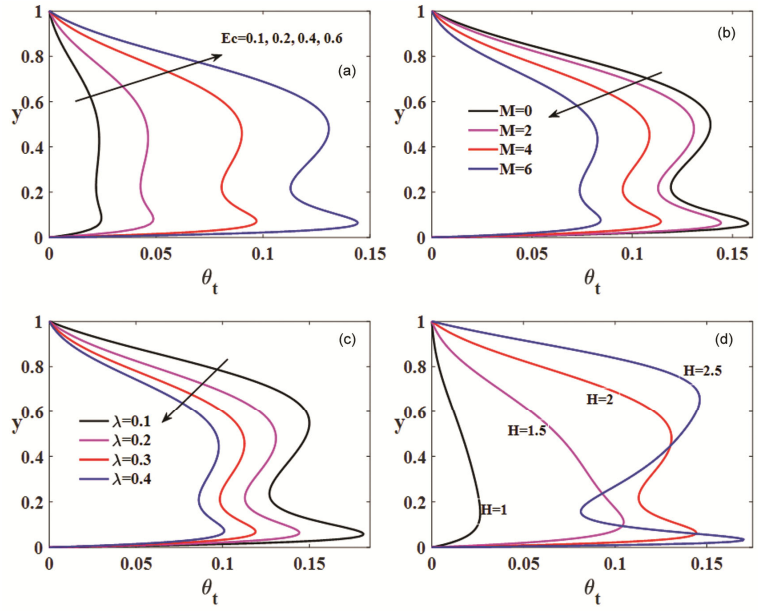

Fig. 6 — (a) Influence of Ec =0.1, 0.2, 0.4, 0.6, on θ_t, (b) influence of M =0, 2, 4, 6, on θ_t, (c) influence of λ =0.1, 0.2, 0.3, 0.4, on θ_t, (d) influence of H =1, 1.5, 2, 2.5, on θ_t.

elucidates the influence of M on temperature distribution θ_t, that is, increasing Hartmann number leads to a decrease in the unsteady temperature of the nanofluid which is due to the Lorentz (retarding) forces (created by the applied magnetic field) slowing down the flow of nanofluid. A similar trend can be found on the profiles of θ_t by varying λ is plotted in Fig. 6(c). From Fig. 6(d), it is clear that there is an increment in the unsteady temperature of nanofluid for the higher values of frequency parameter and the amplitude of profiles of θ_t is also increased with increasing H.

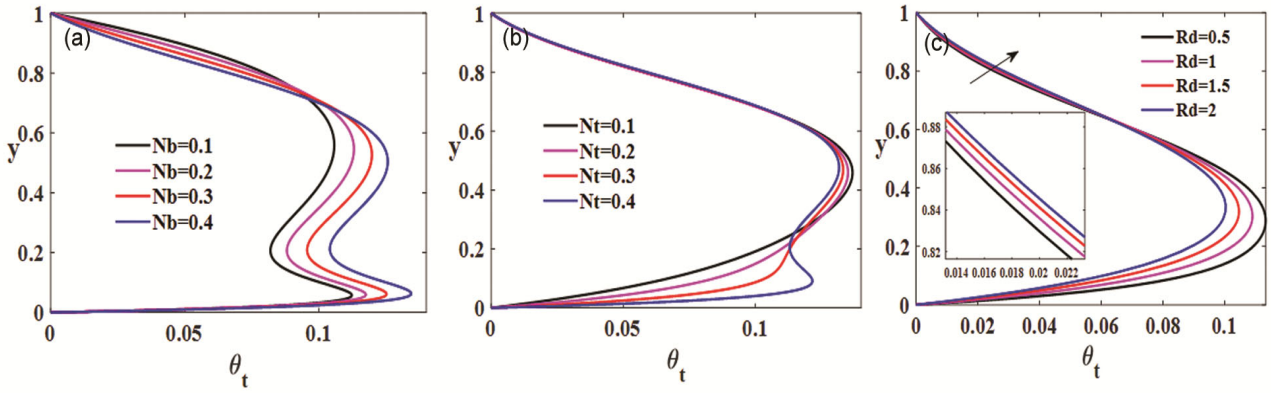

Fig. 7 — (a) Impression of Nb =0.1, 0.2, 0.3, 0.4, on θ_t when $Q=-0.1$, (b) impact of Nt =0.1, 0.2, 0.3, 0.4, on θ_t when $Q=-0.1$, (c) impact of Rd =0.5, 1, 1.5, 2, on θ_t when $Q=-2.5$.

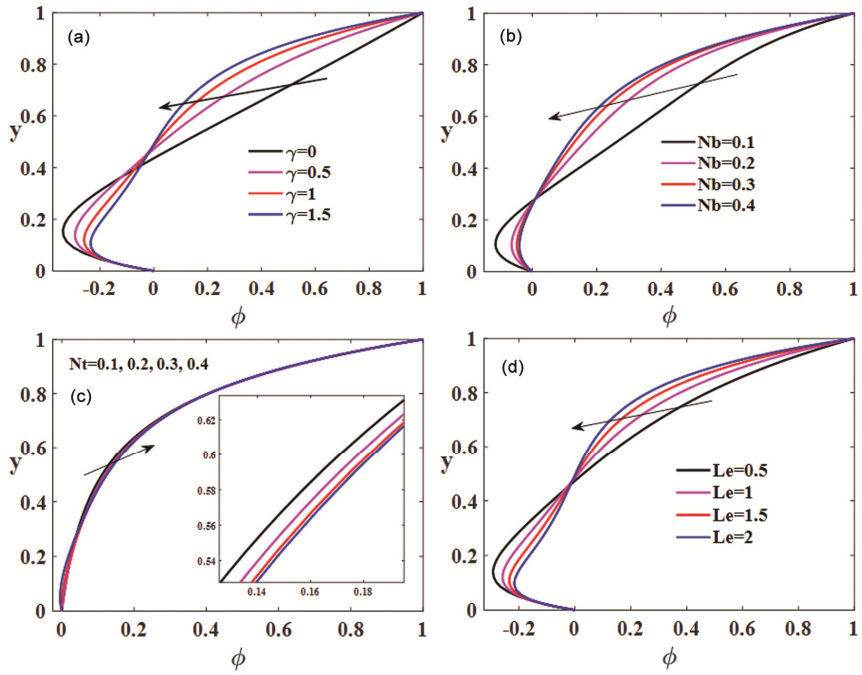

Fig. 8 — (a) Impression of γ =0, 0.5, 1, 1.5, on ϕ when $Q=-0.5$, (b) impact of Nb =0.1, 0.2, 0.3, 0.4, on ϕ when $Q=-2$, (c) impact of Nt =0.1, 0.2, 0.3, 0.4, on ϕ when $Q=-2.5$, (d) impact of Le =0.5, 1, 1.5, 2, on ϕ when $Q=-0.5$.

Figures. 7(a-c) presents the impacts of Nb, Nt, and Rd on θ_t. It is observed from these pictorial outcomes that the distributions of θ_t have an oscillating nature and maximum is near the lower wall. Fig. 7(a) displays the effect of Nb on θ_t, it is clear that there is a rise in the temperature of the nanofluid near the center of the channel with the high values of the Brownian motion parameter. The same observation is noticed from Figs. 7(b,c) by varying thermophoresis parameter and radiation parameter respectively.

Figures. 8(a-d) focused on the impacts of γ, Nb, Nt, and Le on the nanoparticle's concentration profiles. Fig. 8(a) shows that the nanoparticles concentration is decelerating for increasing values of γ. This is because increasing disruptive chemical rate increases the rate of mass transfer which reduces the

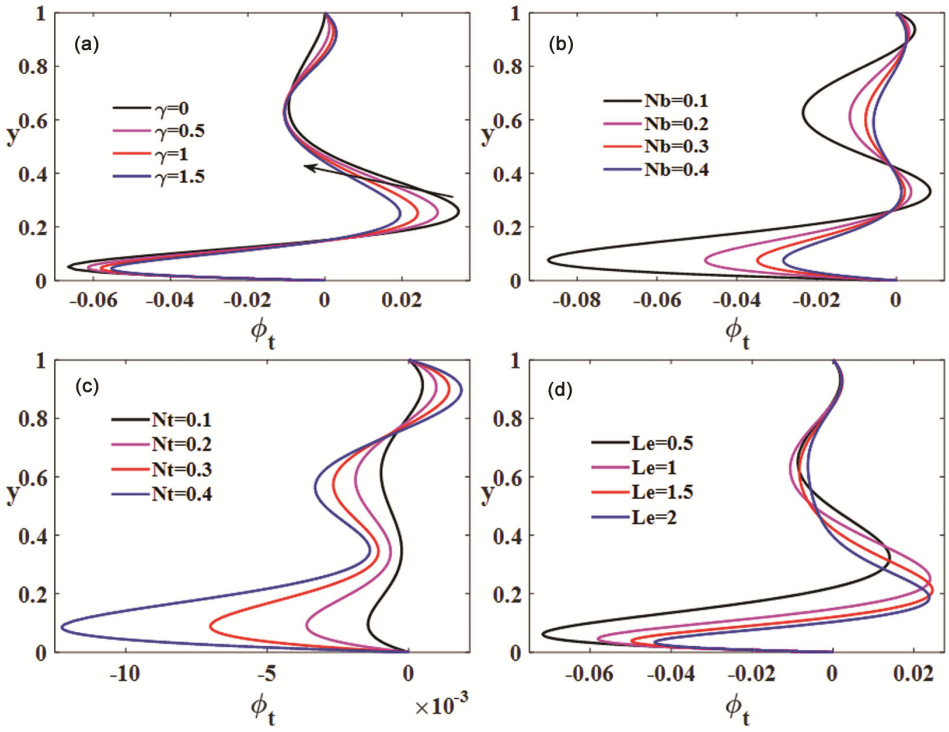

Fig. 9 — (a) Impression of γ =0, 0.5, 1, 1.5, on ϕ_t when $Q=-0.5$, (b) impact of Nb =0.1, 0.2, 0.3, 0.4, on ϕ_t when $Q=-2$, (c) impact of Nt =0.1, 0.2, 0.3, 0.4, on ϕ_t when $Q=-2.5$, (d) impact of Le =0.5, 1, 1.5, 2, on ϕ_t when $Q=-0.5$.

nanoparticle concentration. Fig. 8(b) is delineated to express the influence of Nb on nanoparticles concentration, it is found that the ϕ decreases with rising values of Nb while increasing Nt leads to the gradual improvement of the concentration of nanoparticles, which is portrayed in Fig. 8(c & d) elucidates that increasing Lewis number reduces the concentration of nanoparticles. The reason behind this is the Le is enhancing the mass transfer rate which accelerates the progressive decrease of the concentration of nanoparticles.

The effects of γ, Nb, Nt, and Le on the unsteady concentration of the couple stress nanofluid are displayed in Figs. 9(a-d). Fig. 9(a) elucidates that the unsteady concentration is oscillating with the high values of the chemical reaction parameter. A similar behaviour can be found in Figs. 9(b-c) by varying Brownian motion parameter and thermophoresis parameter respectively. Fig. 9(d) illustrates the impact of Lewis number on ϕ_t. From this figure, one can infer that ϕ_t shows an oscillating character and the maximum is near the bottom wall.

The steady and unsteady heat transfer distributions (Nu_s (*i.e.* θ_0') and Nu_t (i.e. $\varepsilon\theta_1'\exp(it)$)) at the bottom wall ($y=0$) for various values of λ, Nb, Nt, M, Ec, Q (heat source/sink), H and Rd are listed in Table 1. From this table, one can infer that both the steady and unsteady Nusselt numbers are reduced for increasing couple stress parameter, Hartmann number, heat sink ($Q<0$), and Radiation parameter whereas the increasing behaviour can be found for accelerating Brownian motion parameter, thermophoresis parameter, Eckert number, heat source ($Q>0$) and the frequency parameter. The steady and unsteady mass transfer distributions (Sh_s (i.e. ϕ_0') and Sh_t (i.e. $\varepsilon\phi_1'\exp(it)$)) at the bottom wall ($y=0$) for various values of λ, Nb, Nt, M, H and Le are given in Table 2. From the Table 2, it is revealed that both the steady and unsteady Sherwood numbers are increased for the higher values of couple stress parameter, Brownian motion parameter, and the Hartmann number, whereas the trend is reversed for the higher thermophoresis parameter, frequency parameter, and Lewis number.

Table 1 — Distributions of Nu_s (θ_0') and Nu_t ($\varepsilon\theta_1'\exp(it)$) for various values of λ , Nb, Nt, M, EC, Q, H *and* Rd at $Q=-0.5$, $\varepsilon=0.001$, $\lambda=0.2$, $M=2$, $H=2$, $Rd=1$, $\Pr=21$, $Ec=0.6$, $Nb=0.5$, $Nt=0.5$, $\gamma=1$, $Le=1$, $K_1=0.001$, $t=\pi/4$.

λ	Nb	Nt	M	Ec	Q	H	Rd	Nu_s	Nu_t
0.5								7.288166	0.002329
1								6.540175	0.001262
1.5								6.255623	0.000863
2								6.106049	0.000655
	0.1							7.024548	0.003344
	0.2							7.541116	0.003670
	0.3							8.011934	0.003986
	0.4							8.441833	0.004283
		0.1						2.485845	0.000870
		0.2						3.457687	0.001269
		0.3						4.808002	0.001943
		0.4						6.597056	0.003009
			0					9.291085	0.005207
			2					8.836124	0.004557
			4					7.953042	0.003286
			6					7.213318	0.002221
				0.5				8.220420	0.003624
				1				11.705190	0.009093
				1.5				16.467490	0.016764
				2				23.127425	0.026892
					-0.2			14.129214	0.006162
					-0.1			17.182438	0.006816
					0			21.661320	0.007536
					0.1			29.225325	0.008423
					0.2			53.895430	0.011098
						0.5		5.636935	0.000016
						1		5.796324	0.000306
						1.5		6.524836	0.001727
						2		8.836134	0.004557
							0.5	13.914995	0.007962
							1	8.836134	0.004557
							1.5	6.335960	0.002996
							2	4.939916	0.002176

Table 2 — Distributions of Sh_s (ϕ_0') and Sh_t ($\varepsilon\phi_1'\exp(it)$) for various values of λ , Nb, Nt, M, H and Le at $Q=-0.5$, $\varepsilon=0.001$, $\lambda=0.2$, $M=2$, $H=2$, $Rd=1$, $\Pr=21$, $Ec=0.6$, $Nb=0.5$, $Nt=0.5$, $\gamma=1$, $Le=1$, $K_1=0.001$, $t=\pi/4$.

λ	Nb	Nt	M	H	Le	Sh_s	Sh_t
0.5						-4.808885	-0.001536
1						-4.194144	-0.000810
1.5						-3.962706	-0.000547
2						-3.841635	-0.000413
	0.1					-23.367323	-0.010597
	0.2					-12.697479	-0.005968
	0.3					-9.084965	-0.004419
	0.4					-7.240328	-0.003633

(*Contd.*)

Table 2 — Distributions of Sh_s (ϕ_0') and Sh_t ($\varepsilon\phi_1'\exp(it)$) for various values of λ, Nb, Nt, M, H and Le at $Q=-0.5$, $\varepsilon=0.001$, $\lambda=0.2$, $M=2$, $H=2$, $Rd=1$, $\Pr=21$, $Ec=0.6$, $Nb=0.5$, $Nt=0.5$, $\gamma=1$, $Le=1$, $K_1=0.001$, $t=\pi/4$.

λ	Nb	Nt	M	H	Le	Sh_s	Sh_t
		0.1				-0.063548	-0.000045
		0.2				-0.520411	-0.000187
		0.3				-1.492787	-0.000571
		0.4				-3.258856	-0.001446
			0			-6.493170	-0.003638
			2			-6.106345	-0.003147
			4			-5.362602	-0.002215
			6			-4.747428	-0.001463
				0.5		-3.464821	-0.000013
				1		-3.593881	-0.000251
				1.5		-4.187599	-0.001307
				2		-6.106351	-0.003147
					0.5	-5.889459	-0.002968
					1	-6.106351	-0.003147
					1.5	-6.256727	-0.003193
					2	-6.351350	-0.003195

5 Conclusion

The current investigation dealt with the heat (Nusselt number) and mass (Sherwood number) transfer of the magnetohydrodynamic pulsatile flow of a couple stress nanofluid in a channel using the Buongiorno model. The impacts of radiative heat, Ohmic heating, viscous dissipation, Brownian movement, and thermophoresis are considered. The present work is significant in the field of nano-drug delivery, dynamics of physiological fluids, and biomedicines. The numerical outcomes for various parameters are presented by utilizing the shooting process with the support of the Runge-Kutta 4th order procedure. The main conclusions of the current work are listed below:

(i) A strengthening magnetic field slows down the flow and the reverse behavior can be found with the rise in frequency parameter.

(ii) Temperature rises with increasing viscous dissipation whereas the opposite trend can be seen with an escalation in couple stress parameter.

(iii) An increment in Hartmann number and couple stress parameters lead to a decline in the temperature whereas the reverse trend can be identified with a rise in Brownian motion and thermophoresis parameters.

(iv) Temperature is increasing with increase in the heat source, which is due to the heat generation in the fluid, whereas quite opposite behaviour can be found for the high values of the heat sink.

(v) Nusselt number is an increasing function of Brownian motion and thermophoresis parameters while it is a decreasing function of couple stress parameter and radiation parameter.

(vi) Sherwood number decreases with increasing values of thermophoresis and Lewis number whereas the opposite trend can be found with the high values in couple stress parameter and Brownian motion.

References

1 Choi S U S & Eastman J A, *Am Soc Mech Eng Fluids Eng Div FED*, 231 (1995) 99.

2 Assael M J, Antoniadis K D, Wakeham W A & Zhang X, *Int J Heat Mass Transf* ,138 (2019) 597.

3 Hatami M, Hatami J & Ganji D D, *Comput Methods Programs Biomed*, 113 (2014) 632.

4 Pordanjani A H, Aghakhani S, Afrand M, Mahmoudi B, Mahian O & Wongwises S, *Energy Convers Manag*, 198 (2019) 111886.

5 Sheikhpour M, Arabi M, Kasaeian A, Rabei A R & Taherian Z, *Nanotechnol Sci Appl*, 13 (2020) 47.

6 Sheikholeslami M & Chamkha A J, *J Mol Liq*, 225 (2017) 750.

7 Xu H, Fan T & Pop I, *Int Commun Heat Mass Transf*, 44 (2013) 15.

8 Malvandi A & Ganji D D, *Int J Therm Sci*, 84 (2014) 196.

9 Uddin M J, Bég O A, Aziz A & Ismail A I M, *Math Probl Eng*, 2015 (2015) 1.

10 Srinivas S, Vijayalakshmi A, Ramamohan T R & Reddy A S, *J Porous Media,* 17 (2014) 953.

11 Buongiorno J, *J Heat Transfer*, 128 (2006) 240.

12 Nield D A & Kuznetsov A V, *Int J Heat Mass Transf*, 70 (2014) 430.

13 Srinivas S, Vijayalakshmi A, Reddy A S & Ramamohan T R, *Propuls Power Res*, 5 (2016) 134.
14 Makinde O D & Eegunjobi A S, *J Therm Sci Technol*, 12 (2017) JTST0033.
15 Uddin M J, Bég O A & Amin N, *J Magn Magn Mater*, 368 (2014) 252.
16 Chaudhary S & Chouhan K K, *Indian J Pure Appl Phys*, 59 (2021) 559.
17 Rana P, Shehzad S A, Ambreen T & Selim M M, *J Mol Liq*, 334 (2021) 116102.
18 Shamshuddin M D & Eid M R, *J Therm Anal Calorim*, 13 (2021) 1.
19 Srinivasacharya D & Srikanth D, *Comptes Rendus – Mec*, 336 (2008) 820.
20 Zueco J & Beg O A, *Int J Appl Math Mech*, 5 (2009) 1.
21 Adesanya S O, Kareem S O, Falade J A & Arekete S A, *Energy*, 93 (2015) 1239.
22 Misra J C & Chandra S, *J Mech Med Biol*, 18 (2018) 1.
23 Rashad A M, Khan W A, Tlili I & EL-Hakiem A M A, *Indian J Pure Appl Phys*, 57 (2019) 773.
24 Stokes V K, *Phys Fluids*, 11 (1968) 1131.
25 Sithole H, Mondal H, Goqo S, Sibanda P & Motsa S, *Appl Math Comput*, 339 (2018) 820.
26 Salman M R & Abdulhadi A M, *J Phys Conf Ser*, 1032 (2018) 012043.
27 Rosales I G, Duharte G I, Grijalva A L, Danguillecourt O L & Reyes-Nava J, *Heat Transf*, 49 (2020) 4878.
28 Subramaniam C G & Mondal P K, *Phys Fluids*, 32 (2020) 013108.
29 Aziz S, Ahmad I, Ali N & Khan S U, *J Therm Anal Calorim*, 75 (2020) 1.
30 Roja A & Gireesha B J, *Heat Transf*, 49 (2020) 3314.
31 Rajamani S & Reddy A S, *Proc Inst Mech Eng Part E J Process Mech Eng*, 235 (2021) 1895.
32 Stettler J C & Hussain A K M F, *J Fluid Mech*, 170 (1986) 169.
33 Chaturani P & Upadhya V S, *Biorheology*, 15 (1978) 193.
34 Ling S C & Atabek H B, *J Fluid Mech*, 55 (1972) 493.
35 Malathy T & Srinivas S, *Int Commun Heat Mass Transf*, 35 (2008) 681.
36 Datta N, Dalal D C & Mishra S K, *Int J Heat Mass Transf*, 36 (1993) 1783.
37 Srinivas S, Malathy T & Reddy A S, *J King Saud Univ Eng Sci*, 28 (2016) 213.
38 Malathy T, Srinivas S & Reddy A S, *J Porous Media*, 20 (2017) 287.
39 Srinivas S, Kumar C K & Reddy A S, *Nonlinear Anal Model Control*, 23 (2018) 213.
40 Wang C Y, *J Appl Mech*, *Trans ASME*, 38 (1971) 553.
41 Radhakrishnamacharya G & Maiti M K, *J Heat Mass Transf*, 20 (1977) 171.
42 Bestman A R, *Int J Heat Mass Transf*, 25 (1982) 675.
43 Adesanya S O & Makinde O D, *Zeitschrift Fur Naturforsch - Sect A J Phys Sci*, 67 (2012) 647.
44 Ahmed S & Xu H, *Int Commun Heat Mass Transf*, 120 (2021) 105042.
45 Kumar C K, Srinivas S & Reddy A S, *J Mech*, 36 (2020) 535.
46 Ali A, Farooq H, Abbas Z, Bukhari Z & Fatima A, *Sci Rep*, 10 (2020) 1.
47 Venkatesan G & Reddy A S, *Eur Phys J Spec Top*, 230 (2021) 1475.
48 Esfe M H, Bahiraei M, Torabi A & Valadkhani M, *Int Commun Heat Mass Transf*, 120 (2021) 104859.
49 Venkatesan G & Reddy A S, *Heat Transf J*, (2021).
50 Shah Z, Bonyah E, Islam S & Gul T, *AIP Adv*, 9 (2019) 015115.
51 Rashid M, Khan M I, Hayat T, Khan M I & Alsaedi A, *J Mol Liq*, 276 (2019) 441.
52 Hayat T, Bibi A, Yasmin H & Alsaadi F E, *J Therm Sci Eng Appl*, 10 (2018) 051018.
53 Sandhya A, Reddy G V R & Deekshitulu G V S R, *Indian J Pure Appl Phys*, 58 (2020) 548.
54 Vijayaragavan R, Bharathi V & Prakash J, *Indian J Pure Appl Phys*, 59 (2021) 28.
55 Sheikholeslami M & Shehzad S A, *Int J Heat Mass Transf*, 109 (2017) 82.
56 Sheikholeslami M & Rokni H B, *Int J Heat Mass Transf*, 118 (2018) 823.
57 Reddy K V, Reddy M G & Makinde O D, *Period Polytech Mech Eng*, 65 (2021) 151.
58 Shoaib M, Asif M, Raja Z, Touseef M, Awais M, Islam S, Shah Z & Kumam P, *Alexandria Eng J*, 60 (2021) 3605.
59 Ali A, Bukhari Z, Shahzadi G, Abbas Z & Umar M, *Energies,* 14 (2021) 2410.